The rolling elliptical cylinder

Linden, Johan; Källman, Kjell-Mikael; Lindberg, Markus

Published in:
American Journal of Physics

DOI:
10.1119/10.0002362

Published: 01/01/2021

Document Version
Accepted author manuscript

Document License
Unknown

The rolling elliptical cylinder

Johan Lindén* and Kjell-Mikael Källman, and Markus Lindberg

Physics/Faculty of Science and Engineering,

Åbo Akademi University, Turku FI-20500, Finland

(Dated: March 29, 2021)

Abstract

Solving the equations of motion for a cylinder with elliptical cross section rolling down an inclined plane constitutes a rather challenging problem. Using Lagrangian mechanics we have derived the equations of motion analytically and the resulting differential equations are solved numerically. Using a CNC milling machine we manufactured a solid elliptic cylinder and recorded its dynamics using a high-speed video camera for various inclinations of the plane. We compared theory and experiment by extracting the center of mass coordinates and the angular velocity from the video recording. Limits imposed by the support force reaching zero and insufficient friction to prevent slipping were examined both experimentally and theoretically.

I. INTRODUCTION

There are a number of problems in mechanics that students of physics would label as tedious until they have learned the basics of Lagrangian mechanics[1] and suddenly are able to solve surprisingly challenging problems, *e.g.* the double pendulum[2], the multiple Atwood machine[1] or to derive the equations of motion in a rotating frame of reference. On the other hand, there are a number of problems that, despite their simplicity, turn out to be rather challenging to solve. For instance, obtaining the vibrational modes of a drum skin tightly stretched over a frame in the shape of an equilateral triangle[3] is not as easy as when the frame is in the shape of 60°-circular sector.

In this paper we have examined both experimentally and theoretically a problem that definitely belongs to the latter class, namely that of an elliptical cylinder rolling, without slipping, down an inclined plane. Deriving the equations of motion turns out to be a lot nastier than one would expect, in comparison to the trivial case of a cylinder with circular cross section. One of the authors was considering assigning the problem to second-year students in mechanics, until a back-of-the-envelope attempt at solving it indicated that it might not be of appropriate difficulty. To the best of our knowledge the problem has not been addressed before in literature.

II. EXPERIMENT

A cylinder with an elliptic cross section of half axes $a = 2.495 \pm 0.001$ and $b = 1.995 \pm 0.001$ cm was machined from a rod of PVC plastic using a CNC milling machine, Fig. 1. The length of the cylinder was $l = 8.635 \pm 0.001$ cm and mass $M = 0.1962 \pm 0.0001$ kg. Three small beads of different colors were placed symmetrically along the longer axis: one in the center and two on either side of the central one. The cylinder was placed on the higher end of an inclined plane with the longer half axis aligned with the direction of the gravitational force and released. The rolling of the cylinder was filmed using a high-speed video camera operating at a frame rate of 500 fps. The inclination of the plane was varied and two video sequences were recorded for each inclination. A video tracking program[4] was used to track the positions of the beads, frame by frame, in the video sequences. The pixel coordinates of the beads were transformed to physical lengths with the help of a ruler visible in the video.

FIG. 1. (Color Online) The rolling cylinder on the inclined plane. Beads of various colors were used for automatic video tracking.

To minimize solid angle effects, the video filming was done from a distance of ~ 5 m with the lens zoomed to a suitable focal length.

III. THEORY

A. The equations of motion

In order to derive the equations of motions for the cylinder, we will use Lagrange formalism. Fig. 2 illustrates the situation. The inclination of the slope is given by the angle γ. The cylinder is assumed to be rolling without slipping initially. The location of a general mass point m_n of the cylinder is given by the coordinates $x_i^{(n)}(t) = R_i(t) + \sum_{k=1}^{3} r_{ik}(t) s_k^{(n)}$, where $R_i(t)$ defines the position of the center of mass, $r_{ik}(t)$ is the rotation matrix (around the symmetry axis of the cylinder), and $s_k^{(n)}$ the position coordinate of the mass point in relation to the center of mass of the cylinder in a coordinate system fixed to the cylinder. We choose the fixed coordinate system as the principal axis system of the cylinder. The

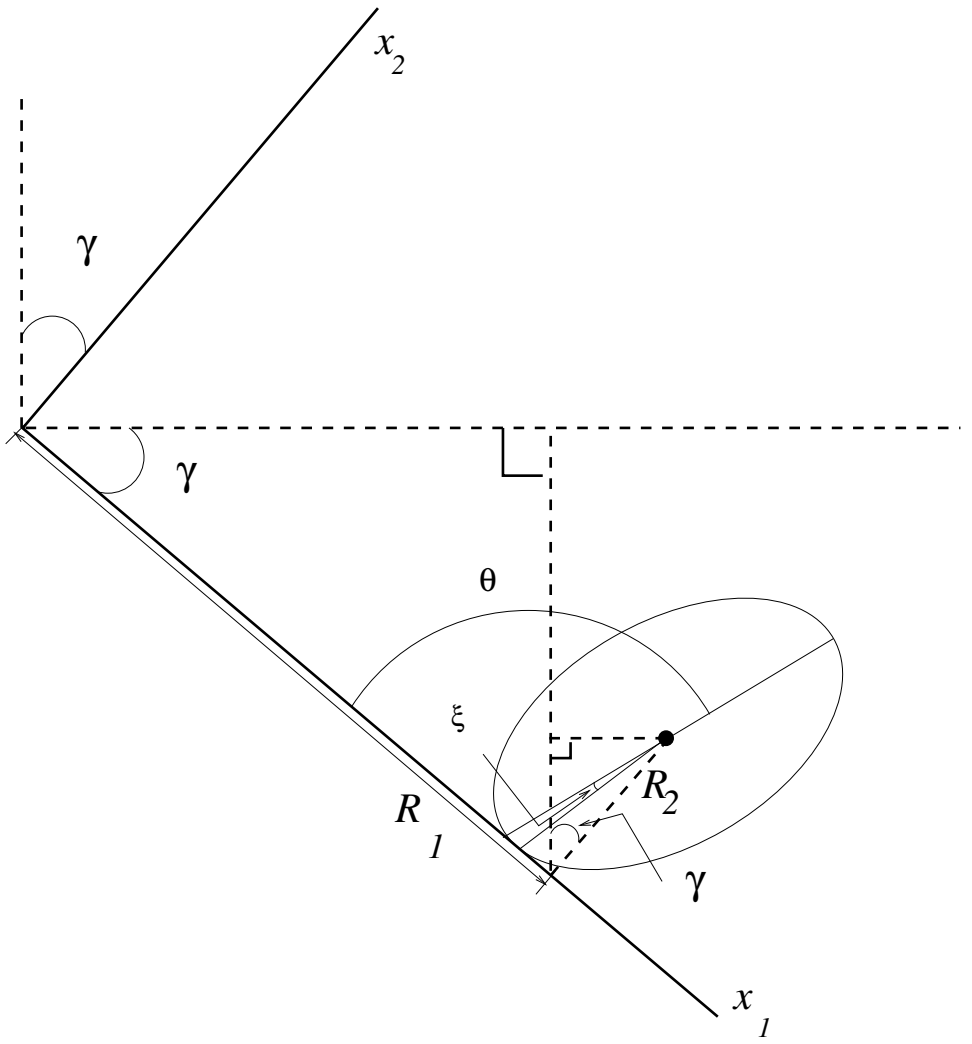

FIG. 2. The rolling cylinder placed in an appropriate coordinate system. The inclination γ is exaggerated.

index i runs from 1 to 3. The index 1 refers to the longer half axis of the ellipse, the index 2 to the shorter half axis, and the index 3 the symmetry axis of the cylinder. The rotation matrix[5] around axis x_3 is given by

$$\mathbf{r}(t) = \begin{pmatrix} \cos\theta(t) & \sin\theta(t) & 0 \\ -\sin\theta(t) & \cos\theta(t) & 0 \\ 0 & 0 & 1 \end{pmatrix}, \tag{1}$$

where $\theta(t)$ is the angle of rotation. The angle $\theta(t) = 0$ refers here to the orientation where the longer half axis is parallel to the axis 1, i.e. along the rolling plane. The typical orientation when the cylinder is released corresponds to $\theta \approx \pi/2$, where the longer half axis

is approximatively parallel to the normal of the rolling plane. The rolling cylinder will have a variable kinetic (T) and potential energy (V). The former consists of two parts, the kinetic energy of the center of mass and the rotational energy:

$$T = \frac{1}{2}M\dot{\vec{R}}^2(t) + \frac{1}{2}I_3\dot{\theta}^2(t), \tag{2}$$

where M is the mass of the cylinder; $\vec{R}(t) = R_1(t)\vec{e}_1 + R_2(t)\vec{e}_2 + R_3(t)\vec{e}_3$ with unit vectors $\vec{e}_1,\ \vec{e}_2,\ \vec{e}_3$ along the three axes and hence $\dot{\vec{R}}^2(t) = \dot{R}_1^2(t) + \dot{R}_2^2(t) + \dot{R}_3^2(t)$; I_3 is the moment of inertia around the symmetry axis; and $\dot{\theta}(t)$ the angular velocity of the cylinder. For an elliptic cylinder with the half axes a and b, $I_3 = \frac{M}{4}(a^2 + b^2) \equiv I$.[6]

The height h of the center of mass below the horizontal plane does not depend on R_3. The height can be expressed with $\gamma,\ R_1$ and R_2 using the geometry drawn in Fig. 2: $h = R_1 \sin\gamma - R_2 \cos\gamma$. As the potential energy $V = -Mgh$ and the Lagrangian is defined as $L = T - V$ we get

$$L = \frac{1}{2}M(\dot{R}_1^2 + \dot{R}_2^2) + \frac{1}{2}I\dot{\theta}^2(t) + Mg(R_1 \sin\gamma - R_2 \cos\gamma), \tag{3}$$

where the index of the moment of inertia has been dropped. Eq. 3 is not yet the proper expression, as r, θ do not qualify as generalized coordinates[1] under pure rolling motion. The rolling cylinder has only one degree of freedom. Let us parametrize a point on the surface of the cylinder with an angle ξ; $\xi \in [0, 2\pi]$, *i.e.* $s_1(\xi) = a\cos\xi$ and $s_2(\xi) = b\sin\xi$, where the cross section of the cylinder is confined within the ellipse $\frac{x_1^2}{a^2} + \frac{x_2^2}{b^2} = 1$. Omitting the direction perpendicular to the cross section, the fixed point on the surface of the cylinder will have the following time-dependent coordinates when rolling:

$$\begin{cases} x_1(\xi, t) = R_1(t) + s_1(\xi)\cos\theta + s_2(\xi)\sin\theta \\ x_2(\xi, t) = R_2(t) - s_1(\xi)\sin\theta + s_2(\xi)\cos\theta, \end{cases} \tag{4}$$

where the rotation matrix 1 has been applied to $s_1(\xi),\ s_2(\xi)$. The cylinder is in contact with the inclined surface at only one point. Thus, for a fixed time t the contact point is identified by a specific value of x_i which is charcterized by the equations $x_2(\xi, t) = 0$ and $\frac{dx_2}{d\xi}(\xi, t) = 0$. As a consequence, the x_i value corresponding to the contact point is a function of time. This leads to

$$\begin{cases} R_2(t) - s_1(\xi)\sin\theta + s_2(\xi)\cos\theta = 0 \\ -s_1'(\xi)\sin\theta + s_2'(\xi)\cos\theta = 0, \end{cases} \tag{5}$$

where the prime denotes taking the derivative with respect to ξ. For rolling motion the distance measured along the perimeter to the point of contact is denoted s. The total "rate of change" for s is $s'(\xi) = \sqrt{s_1'^2 + s_2'^2}$ as infinitesimal increments ds_1 and ds_2 occur along perpendicular axes. Furthermore, as the long axis of the ellipse forms an angle θ with the vertical, the rates of change perpendicular to and parallel with the long axis are $s_2'(\xi) = \sqrt{s_1'^2 + s_2'^2}\sin\theta$ and $s_1'(\xi) = \sqrt{s_1'^2 + s_2'^2}\cos\theta$, respectively.

For rolling motion the distance s accordingly follows from

$$\frac{ds}{dt} = \sqrt{s_1'^2 + s_2'^2}\frac{d\xi}{dt}. \tag{6}$$

This distance must be equal to the distance measured along the x_1 axis, *i.e* $\frac{d}{dt}x_1(\xi,t) = \frac{ds}{dt}$. Taking the left-hand-side derivative, *cf.* Eq. 4 we obtain

$$\frac{d}{dt}x_1(\xi,t) = \dot{R}_1(t) - s_1(\xi)\dot{\theta}\sin\theta + s_2(\xi)\dot{\theta}\cos\theta + [s_1'(\xi)\cos\theta + s_2'(\xi)\sin\theta]\dot{\xi}. \tag{7}$$

The expression in the bracket is equal to $\sqrt{s_1'^2 + s_2'^2}$ and hence the last term simplifies to $\sqrt{s_1'^2 + s_2'^2}\dot{\xi} = \frac{ds}{dt}$, which according to the above observation cancels with the left-hand side of Eq. 7. Therefore,

$$\dot{R}_1(t) - s_1(\xi)\dot{\theta}\sin\theta + s_2(\xi)\dot{\theta}\cos\theta = 0, \tag{8}$$

which the help of Eq. 5 simplifies to

$$\dot{R}_1 = R_2\dot{\theta}, \tag{9}$$

which is in accordance with the usual rolling without slipping condition $v = \omega R$.

Returning to the second expression of Eq. 5 we have $a\sin\theta\sin\xi + b\cos\theta\cos\xi = 0$ or

$$\tan\theta\tan\xi = -\frac{b}{a}, \tag{10}$$

which links the angles θ and ξ together for rolling motion. From the first expression of Eq. 5 we have $R_2(t) = a\cos\xi\sin\theta - b\sin\xi\cos\theta$, the time derivative of which is $\dot{R}_2(t) = (a\cos\xi\cos\theta + b\sin\xi\sin\theta)\dot{\theta}$. From Eq. 8 we have $\dot{R}_1(t) = (a\cos\xi\sin\theta - b\sin\xi\cos\theta)\dot{\theta}$. For the kinetic energy we need $\dot{R}_1^2 + \dot{R}_2^2 = (a^2\cos^2\xi + b^2\sin^2\xi)\dot{\theta}^2$. The ξ dependence can be removed using Eq. 10 leading to

$$\dot{R}_1^2 + \dot{R}_2^2 = \frac{a^4\sin^2\theta + b^4\cos^2\theta}{a^2\sin^2\theta + b^2\cos^2\theta}\dot{\theta}^2. \tag{11}$$

Using Eq. 10 we can obtain expressions for both $\cos\xi$ and $\sin\xi$ as functions of θ enabling us to write R_2 as

$$R_2 = a\sin\theta\frac{1}{\sqrt{1+\frac{b^2}{a^2}\cot^2\theta}} + \frac{b^2}{a}\frac{\cot\theta\cos\theta}{\sqrt{1+\frac{b^2}{a}\cot^2\theta}} = \sqrt{a^2\sin^2\theta + b^2\cos^2\theta}. \tag{12}$$

We also need $R_1(\theta)$ and from Eq. 9 we see that $\frac{dR_1}{d\theta} = R_2$, which suffices for the time being as $R_2(\theta)$ is already known. The Lagrangian can now be written, with θ as the generalized coordinate, as

$$L = \frac{1}{2}M\frac{a^4\sin^2\theta + b^4\cos^2\theta}{a^2\sin^2\theta + b^2\cos^2\theta}\dot{\theta}^2 + \frac{1}{2}I\dot{\theta}^2 + Mg\left(R_1(\theta)\sin\gamma - \sqrt{a^2\sin^2\theta + b^2\cos^2\theta}\cos\gamma\right). \tag{13}$$

For the equations of motion we need $\frac{\partial L}{\partial\dot{\theta}}$ and $\frac{\partial L}{\partial\theta}$. Hence, indeed $\frac{dR_1}{d\theta}$ quite suffices. The two former derivatives are

$$\frac{\partial L}{\partial\dot{\theta}} = M\frac{a^4\sin^2\theta + b^4\cos^2\theta}{a^2\sin^2\theta + b^2\cos^2\theta}\dot{\theta} + I\dot{\theta}, \tag{14}$$

and

$$\frac{\partial L}{\partial\theta} = \frac{1}{2}M\frac{2a^2b^2(a^2-b^2)\sin\theta\cos\theta}{(a^2\sin^2\theta + b^2\cos^2\theta)^2}\dot{\theta}^2 + Mg\left(\sqrt{a^2\sin^2\theta + b^2\cos^2\theta}\sin\gamma - \frac{(a^2-b^2)\sin\theta\cos\theta}{\sqrt{a^2\sin^2\theta + b^2\cos^2\theta}}\cos\gamma\right). \tag{15}$$

Eq. 15 is the right-hand side of the Lagrangian equation of motion

$$\frac{d}{dt}\left(\frac{\partial L}{\partial\dot{\theta}}\right) = \frac{\partial L}{\partial\theta}. \tag{16}$$

For the left-hand side we need the time derivative of Eq. 14

$$\frac{d}{dt}\frac{\partial L}{\partial\dot{\theta}} = M\frac{a^4\sin^2\theta + b^4\cos^2\theta}{a^2\sin^2\theta + b^2\cos^2\theta}\ddot{\theta} + I\ddot{\theta} + M\frac{2a^2b^2(a^2-b^2)\sin\theta\cos\theta}{(a^2\sin^2\theta + b^2\cos^2\theta)^2}\dot{\theta}^2. \tag{17}$$

Upon inserting Eqs. 17 and 15 into Eq. 16 the equation of motion becomes

$$\begin{aligned} M\frac{a^4\sin^2\theta + b^4\cos^2\theta}{a^2\sin^2\theta + b^2\cos^2\theta}\ddot{\theta} + I\ddot{\theta} = \quad & Mg\left(\sqrt{a^2\sin^2\theta + b^2\cos^2\theta}\sin\gamma - \frac{(a^2-b^2)\sin\theta\cos\theta}{\sqrt{a^2\sin^2\theta + b^2\cos^2\theta}}\cos\gamma\right) \\ & -\frac{1}{2}M\frac{2a^2b^2(a^2-b^2)\sin\theta\cos\theta}{(a^2\sin^2\theta + b^2\cos^2\theta)^2}\dot{\theta}^2 \end{aligned} \tag{18}$$

which is reduced to the trivial case

$$Ma^2\ddot{\theta} + I\ddot{\theta} = Mga\sin\gamma \tag{19}$$

of a rolling circular cylinder when $a = b$.

A complete solution requires the coordinates (R_1, R_2) of the center of mass. The first coordinate is obtained from an incomplete elliptic integral

$$R_1(\theta) = \int_{\theta_0}^{\theta} d\theta' \sqrt{a^2 \sin^2\theta' + b^2 \cos^2\theta'}, \tag{20}$$

while R_2 is explicitly in Eq. 12. The angle θ_0 refers to the orientation of the cylinder the time of release. Assuming $a \geq b$ we have in the standard notation

$$R_1(\theta) = a \left[E\left(\theta + \pi/2 \mid \frac{a^2 - b^2}{a^2}\right) \; - \; E\left(\theta_0 + \pi/2 \mid \frac{a^2 - b^2}{a^2}\right)\right], \tag{21}$$

where $E(x \mid k)$ is the incomplete elliptic integral of the second kind,

$$E(x \mid k) \equiv \int_0^x dx' \sqrt{1 - k \sin^2(x')}. \tag{22}$$

IV. RESULTS AND DISCUSSION

Eqs. 18 and 12 were first solved numerically to obtain $\theta, \dot{\theta}$ and R_2 using a Fortran program dedicated to this problem. For details, see the appendix. The mass M could be removed from Eq. 18, as it multiplies all the terms including the moment of inertia. Instead of using the analytical expression for the elliptic integral of Eq. 20, Eq. 9 was used for obtaining R_1 numerically. The total energy of the cylinder was also evaluated for each simulation by forming $E = T + V$ using the Lagrangian of Eq. 13. A typical variation in E of less than ± 10 ppm was due to the finite time step size used in the simulation.

From the position of the central bead inserted into the cylinder the (R_1, R_2) coordinates of the mass center were determined from the video material, *cf.* Fig. 3. Due to the inclination, the pixel coordinates had to be rotated using matrix 1 to obtain coordinates directed along the plane and perpendicular to it. The two other beads were originally used for observing the rotation angle θ and the angular velocity $\dot{\theta}$. However, Eq. 9 can easily be used for extracting the angular velocity from the data, as $\dot{\theta} = \dot{R}_1/R_2$, where $\dot{R}_1$ was obtained as $(R_1^{i+1} - R_1^i)/\Delta t$, with $\Delta t = 2.0$ ms according to the video frame rate. The experimentally obtained time dependencies for R_1, R_2 and $\dot{\theta}$ were compared with the theoretical models obtained from Eqs. 12, 20 and 18.

The experimental data and curves obtained from the theoretical model can be plotted together in order to see how well they match. However, before doing it there were three parameters that had to be determined: The angle γ, the initial inclination of the cylinder θ_0,

and finally a possible time difference δt between the experimental data and the theoretical curve. The inclination γ was measured when setting up the experiment, but with an accuracy of merely $\pm 0.5^\circ$, while θ_0 could be estimated directly from the video. The timing between the data and the theoretical curve had to be adjusted typically by less than 0.1 s. In Fig. 3

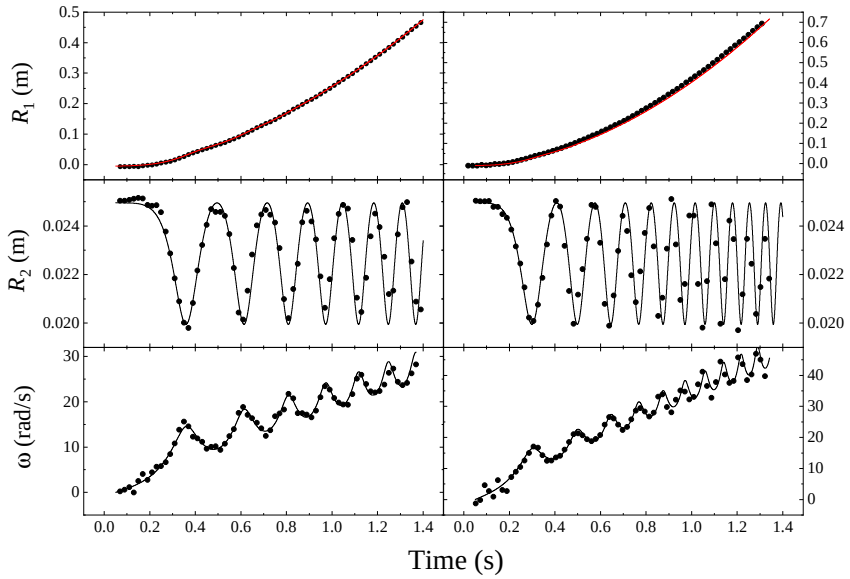

FIG. 3. (Color Online) The time evolution of the angular velocity and coordinates R_1, R_2 measured along the inclined plane for an inclination of 3.35° (left column) and 6.5° (right column). The theoretical curves were obtained by numerically solving the equations of motion, see text. The experimental data (bullets) were obtained from the video tracker. The statistical errors do not exceed the size of the symbols for R_1 and are approximately twice the symbol size for R_2 and ω.

the coordinates are plotted as a function of time, with the nominal inclinations $\gamma = 3^\circ$ and 6°. In the analysis, the values used were $\gamma = 3.35 \pm 0.05^\circ$, $\theta_0 = 93.0 \pm 0.1^\circ$, $\delta t = 0.07 \pm 0.01$ s and $\gamma = 6.50 \pm 0.05^\circ$, $\theta_0 = 90.1 \pm 0.1^\circ$, $\delta t = 0.03 \pm 0.01$ s, respectively for the two experiments. The data were cut when the cylinder has rolled for $t \approx 1.4$ s. The cylinder had reached 45 cm down the plane at $\gamma = 3.35 \pm 0.05^\circ$ and the oscillatory behavior of coordinate R_2, Fig. 3 began to deviate qualitatively from the theoretical behavior at this point. Up to $t = 1.4$ s the agreement between theory and experiment is fairly good. For the steeper slope deviation occurs already at $t \approx 0.8$ s.

The deviation from the ordinary rolling behavior can be explored by examining the sup-

port forces, i.e. the normal force N between the plane and the cylinder, and the static friction force f along the plane, required to achieve the observed acceleration of the mass center $\ddot{R}_1\vec{e}_1 + \ddot{R}_2\vec{e}_2$ and the angular acceleration $\ddot{\theta}$. The normal force is obtained from normal component of Newton's second law by assuming that the plane gives rise to a normal component of the support force on the cylinder at the point of contact giving

$$N = M(\ddot{R}_2 + g\cos\gamma). \tag{23}$$

Similarly, the in-plane component of the support force, called static friction force f, acts on the cylinder at the point of contact, and is expressed by

$$f = M(\ddot{R}_1 - g\sin\gamma). \tag{24}$$

The friction forces caused by supporting surfaces are essentially impossible to describe applying fundamental forces as the surface roughness plays a fundamental role. The simplest possible phenomenological model for the friction force is constructed using the static friction coefficient defined by $\mu = f/N$. Observations show that the maximal friction coefficient is obtained when the force drawing the piece of material along the surface is just at the threshold of starting to move. Once moving, the friction coefficient is smaller. This observed property sets a limit to how large in-plane support forces can be obtained in reality. The problems related to the friction force are demonstrated by the fact that the simulations give a time-dependent friction coefficient which depends on the way the cylinder is released. The friction coefficient is therefore not a property of the plane surface and the cylinder surface in static contact. A quantitative description of it would require detailed knowledge of the surface roughness and the molecular forces at both surfaces.

Experimentally the coefficient of static friction was determined by putting the cylinder with the symmetry axis parallel with the slope and slowly increasing the inclination. When slipping occurred the inclination angle was noted and the coefficient was obtained as $\mu = \tan\gamma$. As the critical angle was $\sim 27^\circ$, corresponding to $\mu \approx 0.5$. This is the maximum value of the friction coefficient that the real system observed by us, can produce. Consequently, when the friction coefficient required by the simulation exceeds 0.5, simulated motion and the real motion are bound to deviate.

In our system, there is no stickiness in the contact between the cylinder and the plane. Consequently, the normal support force cannot be negative. These observed properties mean

that our simulation cannot describe the physical motion if the required support forces exceed the limits set by the physical contact between the real cylinder and the plane.

However, we should also examine the expression for angular acceleration $\tau = I\ddot{\theta}$, where the torque τ depends on both support force components N and f. The lever for the friction is simply R_2, while for the support force N the lever is $x_1 - R_1$, which is zero when θ is a multiple of $\pi/2$. Using these quantities we have

$$\tau = R_2 f - (x_1 - R_1)N = R_2 f - (a\cos\xi\cos\theta + b\sin\xi\sin\theta)N, \tag{25}$$

where the last step followed from Eq. 4. Putting $\tau = I\ddot{\theta}$, the friction required for the rolling is $f = \frac{I\ddot{\theta}}{R_2} + N\cos\xi\cos\theta(a^2 - b^2)/(aR_2)$, where Eq. 10 was used. Despite the fact that the two expressions for the friction look different, they produce exactly the same result when evaluated numerically. When the simulation requires a coefficient of static friction above 0.5, to maintain the no-slip condition, the cylinder most likely begins to slip in the experimental setup. For an inclination of 3.35° this happens soon after $t = 1.8$ s, and slightly later the theoretical value for μ would soar above unity. Almost at the same time the support force reaches zero and the cylinder would for the first time become airborne. In Fig. 4 the theoretical values for the normal force and the friction are shown for the case where $\gamma = 3.35°$. Points presented in red indicate where the normal force is negative or a friction coefficient larger than 0.5 would be needed to achieve the theoretically determined friction force.

It is noteworthy that the friction changes direction regularly. Due to the oscillatory behavior of $\dot{\theta}$ and $\dot{R}_1$, both the accelerations $\ddot{\theta}$ and $\ddot{R}_1$ attain positive and negative values, explaining the oscillations of the friction. Naturally, both accelerations oscillate around a constant value, which for $\ddot{R}_1$ is $g\sin\gamma$. The oscillations which grow increasingly more rapid result in a friction force which grows with time. This is in sharp contrast to that obtained for a circular cylinder for which f is constant.

The reason that the experimental coordinates begin to deviate already at $t = 1.4$ s could be related to cumulated effect of rolling resistance which is not included in the model simulated. Nevertheless, the experimental data corresponds well to the theoretical model of rolling without slipping up to $t = 1.4$ s for $\gamma = 3.35°$ and $t = 0.8$ s for $\gamma = 6.5°$. The angular velocity illustrates this rather well also, Fig. 3. It is also interesting to observe the motion of the off-center beads. The white bead located 17 mm from the center of mass offered the

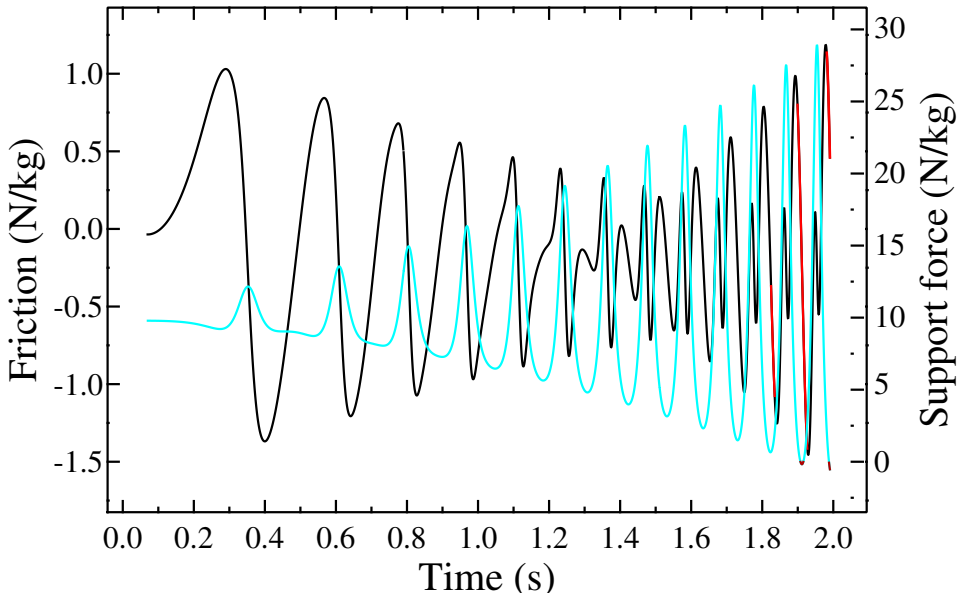

FIG. 4. (Color Online) Calculated values for the normal force N (cyan) and static friction f (black), given in units force per mass, as the cylinder rolls down a plane with an inclination of 3.35°. Regions where either force violates the experimental conditions, see text, are highlighted in red.

best contrast in the black and white video material. The coordinates are presented in Fig. 5. The theoretical coordinates were obtained as $x_1 = R_1 + d\sin\theta$ and $x_2 = R_2 + d\cos\theta$, where $d = 17$ mm is the distance from the mass center to the white bead.

Upon increasing the inclination of the plane, similar results are obtained, except that the time until deviation from the pure rolling motion occurs is reduced, decreasing the number of revolutions the cylinder undergoes before slipping occurs and/or the cylinder loses contact with the track. For larger inclination angles it was also possible to observe the point were the cylinder became airborne from the video material marking the definite failure of the model.

Future experiments should probably involve smaller inclinations to evaluate the role of rolling resistance. A cylinder of larger average diameter should be used. This would increase the time until slipping occurs and improve the experimental resolution. For an inclination of 3.5° slipping seems to occur before the cylinder becomes airborne according to the simulation. It would be interesting to see if the opposite case is possible, where slipping has not yet occurred when the cylinder becomes airborne for the first time. The first jump of the cylinder

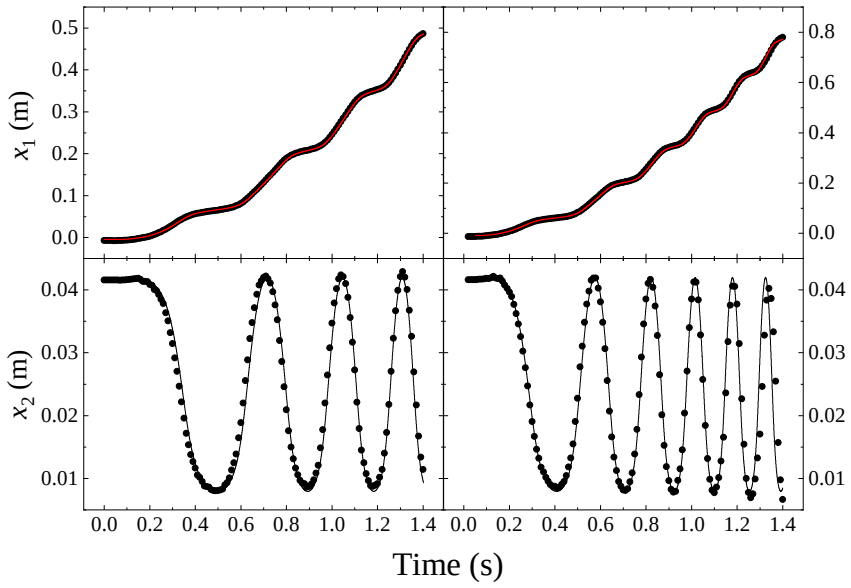

FIG. 5. (Color Online) The x_1 and x_2 coordinates vs. time for the white bead, when the cylinder is rolling down the 3.35° (left column) and 6.50° (right column) inclination. Wiggles due to the motion of the off-center position are well visible. The theoretical curve was obtained by solving the equations of motion. Statistical errors do not exceed (x_1) or are twice (x_2) the size of the symbols.

could then be considered dissipation free and possible to model with a small extension of the program. However, the main goal of this paper (to derive the equations of motion for a rolling elliptic cylinder) was achieved.

As a practical mechanical application the formalism outlined here might be useful for studying the support forces acting on deformed (and non-compressible) wheels, e.g. train or streetcar wheels. For this purpose other deformations than an elliptical distortion of the wheel should also be considered.

V. CONCLUSIONS

We have studied both theoretically and experimentally the rolling of an elliptic cylinder. The equations of motions were derived using Lagrangian formalism, but solving the resulting (rather daunting) differential equations was not possible analytically. Instead we resorted to numerical methods. The motion of the cylinder could be described by the coordinates

of its center of mass, its angular velocity, or position any off-center mass point. All these experimentally obtained values agreed well with the numerical solutions. The regime of pure rolling motion was theoretically determined from the support force between the inclined plane and the rolling cylinder, as well as from the value of static friction required to achieve the rotation and the motion of the mass center. This led to two different criteria for ideal rolling motion. However, they both gave approximately the same time limitation for the end of the rolling motion. Numerically the solutions to the equations seemed rather stable and the total energy of the system remained constant to within 10 ppm. The correctness of the model is also supported by the fact the the force of friction determined from the angular acceleration and the mass center acceleration were identical within a few tens of ppm.

ACKNOWLEDGMENTS

Mr. Alf Hermanson is acknowledged for his help in recording the high-speed videos. Dr. Torbjörn Björkman is acknowledged for valuable discussions.

APPENDIX A

In this appendix the numerical solution of Eq. 18 is outlined. The program solving the differential equations was written in Fortran 77 and compiled using the gfortran compiler on a a ten-year-old Asus N61JA laptop with Ubuntu 18.04 as operating system. A time step of 25 μs was used when solving the differential equations.

As the time dependences of the coordinates are rather slow, and the resulting quasiperiodic functions rather smooth, a simple low-order Euler method[7] was chosen for solving Eq. 18. In most cases higher order methods are needed and recommended for numerical solutions. The first step was to formally solve for $\ddot{\theta}$, and inserting the initial values for γ, $g = 9.81$ m/s^2 and $\theta, \dot{\theta}$. Using a time step of dt, the latter two quantities were updated as $\dot{\theta} \to \dot{\theta} + dt\ddot{\theta}$ and $\theta \to \theta + dt\dot{\theta}$ followed by a repetition of the first step, until the total time amounted to ~ 2.0 s. For each step the sum of kinetic and potential energy was calculated.

Another way to obtain numerical values, is to directly use the conservation of energy $E = T + V$. The Lagrange equation of motion leads to the result that the quantity

$$\frac{1}{2}M\frac{a^4\sin^2\theta + b^4\cos^2\theta}{a^2\sin^2\theta + b^2\cos^2\theta}\dot{\theta}^2 + \frac{1}{2}I\dot{\theta}^2 \;-\; Mg\left(R_1(\theta)\sin\gamma - \sqrt{a^2\sin^2\theta + b^2\cos^2\theta}\cos\gamma\right). \quad (26)$$

is a constant of motion we call energy E when $\theta = \theta(t)$ satisfies (18). Consequently we have

an equation of motion for $\theta(t)$ in the form

$$\frac{1}{2}M\frac{a^4\sin^2\theta(t)+b^4\cos^2\theta(t)}{a^2\sin^2\theta(t)+b^2\cos^2\theta(t)}\dot{\theta}(t)^2+\frac{1}{2}I\dot{\theta}(t)^2-Mg\left(R_1(\theta(t))\sin\gamma-\sqrt{a^2\sin^2\theta(t)+b^2\cos^2\theta(t)}\cos\gamma\right)=E. \tag{27}$$

This is a differential equation of the order 1 for $\theta(t)$, that can be solved numerically. A formal solution for the equation of motion can be presented in form of an integral

$$t-t_0=\int_{\theta_0}^{\theta}d\theta'\sqrt{\frac{\frac{1}{2}\frac{a^4\sin^2\theta'+b^4\cos^2\theta'}{a^2\sin^2\theta'+b^2\cos^2\theta'}+\frac{1}{8}(a^2+b^2)}{E/M+g\left(R_1(\theta')\sin\gamma-\sqrt{a^2\sin^2\theta'+b^2\cos^2\theta'}\cos\gamma\right)}}. \tag{28}$$

Note that E/M is independent of M. The equation can be solved numerically using various methods. Its drawback is that $R_1(\theta(t))$ must be evaluated at each step of the integration. The solution gives $t-t_0$ as a function of θ. To obtain θ as a function of t, this relation must still be inverted after the integral has been evaluated. However, for numerical purposes calculating the time for given values of θ is equally feasible, see Appendix B.

APPENDIX B

A numerical solution of the integral of Eq. 28 is presented in this appendix and compared with the results obtained from Eq. 18. First we evaluated the incomplete elliptical integral for $R_1(\theta)$ and tabulated the results for various values of θ. A step size of 0.0005 radians was used and the integrals were solved using a simple midpoint rectangular method. After this Eq. 28 was solved using the same method and identical step size, resulting in a data set of time vs. θ. Upon inclusion of the numerical integration routine the run time of the Fortran program approximately doubled, but was still no more than a few tens of seconds on the laptop. By plotting the resulting θ vs. time data, obtained using the two methods presented in this paper in the same graph, a visual inspection indicates that they are almost identical, Fig. 6. However, after calculating 6.5 revolutions or 40 radians corresponding to 1.88 s on a slope of 3.5° the difference in the θ angle was 0.15 rad between the methods. By decreasing the step sizes of the angle and the time with a factor of four the difference halved. It is probable that higher order numerical integration methods would decrease the difference faster. Nevertheless based on the θ vs. t dependence it is not possible to say which method is more economical from a computing point of view. Eq. 28 has the advantage of automatically conserving the total mechanical energy, as it is basically a first integral of Newtons second law.

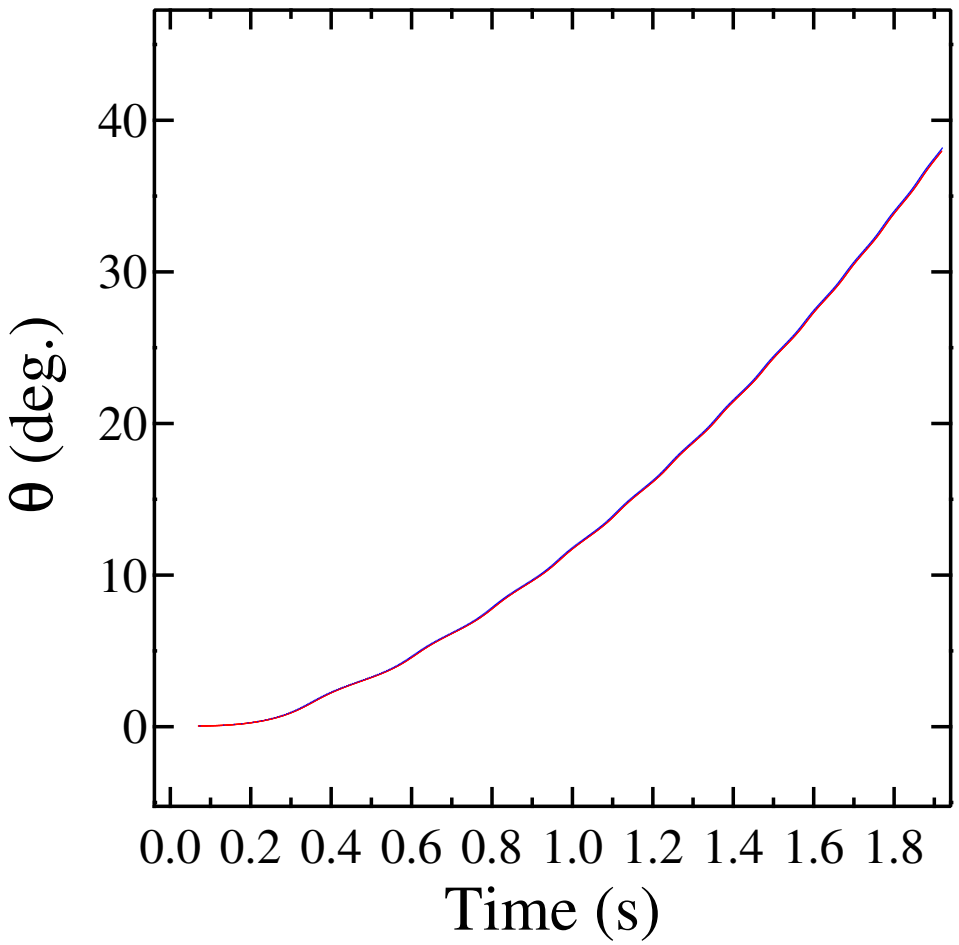

FIG. 6. (Color Online) Simulated values for the angle θ obtained using numerical solutions of Eq. 18 (red) and Eq. 28 (blue). As the curves are practically on top of each other the resulting plot looks purple.

---

* jlinden@abo.fi

[1] G.R. Fowles and G.L. Cassiday in *Analytical Mechanics, 6th ed.* pp. 391-404 (Saunders 1990).

[2] Keith R. Symon in *Mechanics, 3rd ed.* Problem 9.11 p. 398 (Adison-Wesley 1971).

[3] D.G. Christopherson *Note on the Vibration of Membranes*, Quart. J. Math. **11**, 65 (1940).

[4] https://physlets.org/tracker/ (Downloaded May 2019)

[5] G. Arfken in *Mathematical methods for physicists, 3rd ed.* p. 196 (Academic Press 1985).

[6] Dwight E. Gray ed. in *American Institute of Physics Handbook, 3rd ed.* p. 2-41 (McGraw-Hill 1972).

[7] Anthony Ralston,"Runge-Kutta Methods with Minimum Error Bounds". Math. Comput. **16** 431 (1962).